RSC Advances

Preparation of Ti mesh supported N-S-C-tridoped TiO2 nanosheets to achieve high utilization of optical energy for photocatalytic degradation of norfloxacin

Journal:	*RSC Advances*
Manuscript ID	RA-ART-12-2015-027639.R1
Article Type:	Paper
Date Submitted by the Author:	26-Jan-2016
Complete List of Authors:	Zhang, Xiaoyun; Heilongjiang University Li, Dong; Heilongjiang University Wan, Jiafeng; Heilongjiang University, Yu, Xiujuan; Heilongjiang University, Environmental Science and Engineering
Subject area & keyword:	Photocatalysis < Catalysis

Preparation of Ti mesh supported N-S-C-tridoped TiO_2 nanosheets to achieve high utilization of optical energy for photocatalytic degradation of norfloxacin

Xiaoyun Zhang ,[a] Dong Li, [a] Jiafeng Wan ,[a,b,*] Xiujuan Yu [a,b,*]

[a] Department of Environmental Science and Engineering, Heilongjiang University, Xuefu Road 74, Nangang District, Harbin 150080, Heilongjiang Province, PR China

[b] Key Laboratory of Chemical Engineering Process & Technology for High-efficiency Conversion, Harbin, College of Heilongjiang Province, P.R. China.

*Corresponding author Address: Department of Environmental Science and Engineering, Heilongjiang University, Xuefu Road 74, Nangang District, Harbin 150080, Heilongjiang Province, PR China

Phone: +86 451 86608549

Fax: +86 451 86413259

E-mail: wanjiafeng@hlju.edu.cn; yuxiujuan@hlju.edu.cn

Abstract

The Ti meshes supported N-S-C-tridoped TiO_2 nanosheets (N-S-C-/TiO_2/TMs) catalysts were successfully fabricated by the one-step in situ hydrothermal synthesis method, and then used for photocatalytic degradation of norfloxacin. The prepared samples were characterized by X-ray photoelectron spectroscopy (XPS), scanning electrons microscopy (SEM), X-ray diffraction (XRD), and UV-vis diffuse reflectance spectra (DRS). The results showed that the N, S and C transfered into the lattice of TiO_2 and improved the visible-light response of TiO_2/TM. The degradation of norfloxacin by trilaminar Ti meshes supported N-S-C/TiO_2 (3-N-S-C/TiO_2/TMs) catalysts were 92%, much higher than that of 3-TiO_2/TMs. Furthermore, the photocatalytic performances of 3-TiO_2/TMs and equiponderant one Ti foil supported TiO_2 (1-TiO_2/TF) were also investigated. The experimental results demonstrated that the characteristic three-dimensional (3D) arrays and porous structure of 3-TiO_2/TMs significantly enhanced the photon utilization during the degradation reaction, which induced a much higher degradation efficiency of 55% than that of equiponderant 1-TiO_2/TF (23%) in 120 min.

1. Introduction

The release of antibiotics into the aquatic environment has increased significantly in recent years.[1] Among the antibiotic drugs, the fluoroquinolone group, which is derived from nalidixic acid, is probably the most important class of synthetic antibiotics.[2] Norfloxacin [1-ethyl-6-fluoro-1, 4-dihydro-4-oxo-7-(1-piperazinyl)-3-quinolinecarboxylic acid] is a representative member of fluoroquinolone family and used in a wide range of gastrointestinal, urinary, respiratory tract, skin and intra-abdominal infections.[3-5] However, due to the widespread usage of norfloxacin in everyday life, large amounts of norfloxacin are released to the aquatic environment through domestic wastewater, hospital sewages and industrial discharges.[6,7] So far, norfloxacin has been detected in various water sources, including sewage treatment plant effluents, surface water, seawater, groundwater and drinking water.[8-10] Among many processes proposed and/or being developed for the removal of norfloxacin, biodegradation has received the greatest attention. However, the deficiency of inefficiency exists in the traditional biological treatment. Therefore, the techniques resulting in efficient or complete degradation are required in present.

Recently, the semiconductor photocatalysis oxidation technology is considered as relatively efficient technique with key advantages of enduring stability and complete degradation.[11] Among the semiconductor photocatalysts, TiO_2 is one of the mostly used photocatalyst due to its low toxicity, high efficiency, excellent physico-chemical stability and low costs.[12-15] Unfortunately, the large band gap and low quantum yield of TiO_2 catalyst significantly restrain its photocatalytic activity. In order to effectively enhance the photocatalytic performance of TiO_2, intensive research efforts have been focused on the modification of TiO_2 with various doping agents.[16-19] Among these efforts, several studies have reported that N, S and C tridoping could efficiently improve the visible light response and quantum efficiency of TiO_2, thus enhancing the photocatalytic activity.[20-22] Generally, N-S-C-tridoped TiO_2 photocatalyst is always used as a powder or as a film for photocatalytic degradation. However, the highly dispersed N-S-C-tridoped TiO_2 powder must be recycled after the photocatalytic reaction in a suspension reactor. The post-treatment process requires a solid–liquid separation stage which will increase the difficulty in operation and cost.[23] The immobilization of N-S-C-tridoped TiO_2 film on a appropriate substrate can efficiently minimize post-treatment process and improve the degradation kinetics in the presence of a suitable external bias.[24] Efforts have been made to immobilize N-S-C-tridoped TiO_2 on Ti foil for photoelectrocatalytic degradation of methyl orange.[25] However, the use of Ti in the form of a foil can be expensive and wasteful. For instance, Liao et al. found that when the TiO_2/Ti foil weighs 0.4 g, TiO_2/Ti mesh with the same apparent area weighs only 0.2 g.[26] That is, two TiO_2/Ti meshes or one TiO_2/Ti foil, which have the same apparent area, can be obtained by using the equivalent weight of metallic Ti.

Moreover, Ti mesh supported TiO_2 nanosheets present extraordinary advantages as compared to Ti foil supported TiO_2 nanosheets on preparing immobilized photocatalyts. First, unlike planar Ti foil where nanosheets are grown vertically in two-dimensional (2D) arrays, TiO_2 nanosheets can be formed in all directions over a Ti wire in three-dimensional (3D) arrays.[27,28] Therefore, loss of photons attributed to scattering effects in the liquid can potentially be minimized since the nanosheets can absorb reflected and/or refracted light. Second, owning to the porous structure of Ti mesh, flowing pollutant can easily diffuse/transport through those holes, thus enhancing the degradation efficiency.[29] Finally, the network structure can enhance the light utilization of catalysts, because polylaminate catalysts can function simultaneously when irradiation is applied, which is beneficial to its potential applications in practical water purification.

In this paper, N-S-C-tridoped TiO_2 nanosheets photocatalysts were prepared on the surface of Ti mesh by a simple hydrothermal method in the mixed aqueous solution of sodium hydroxide and cystine, then followed by photocatalytic degradation of norfloxacin under visible light irradiation. In addition, a comparative analysis of the photocatalytic activity of TiO_2 nanosheets formed over Ti meshes and equiponderant foil was also investigated.

2. Experimental

2.1 Synthesis of Ti mesh supported N-S-C-tridoped TiO_2 nanosheets photocatalyst

Ti mesh (0.2 g, 20×30 mm^2, 80 mesh, 0.11 mm thick, purity 99.7%) was used as titanium source. The Ti mesh supported N-S-C-tridoped TiO_2 nanosheets (N-S-C/TiO_2/TM) catalyst was prepared by a simple one-step hydrothermal method in the mixture of sodium hydroxide and cystine. Before hydrothermal reaction, Ti mesh was polished in the mixed acid solution of HF, HNO_3 and H_2O with the volume ratio of 1:4:5. Then the polished Ti mesh was sonicated by ethanol, acetone and deionized water for 15 min, respectively. Subsequently, the cleaned Ti mesh was transferred into the teflon-lined stainless steel autoclave, which containing 30 mL mixed solution of 6 mol L^{-1} NaOH and 0.15 mol L^{-1} cystine. The sealed autoclave was kept at 170°C for 35 h. After the hydrothermal treatment,

the prepared sample was immersed in 0.3 mol L^{-1} HCl for 1 h, the Na^+ of sample was exchanged with H^+. At last it was calcinated at 450 °C for 3 h to convert into N-S-C-tridoped TiO_2 nanosheets. To investigate the influence of different Ti substrates on the photocatalytic activity of TiO_2. Three Ti meshes and equiponderant one foil (0.6 g, 20×30 mm^2, 0.11 mm thick, purity 99.7%) were used as supports for synthesis of pure TiO_2. Except for the removal of cystine during the hydrothermal process, the synthesis method of TiO_2 was identical with that of N-S-C/TiO_2/TM sample.

2.2 Characterization

X-ray photoelectron spectroscopy (XPS, Kratos-AXIS UL TRA DLD, Al Ka X-ray source) was conducted to characterize the chemical states of tridoped carbon, nitrogen and sulfur atoms in the N-S-C/TiO_2/TM sample. The morphologies of N-S-C/TiO_2/TM sample were characterized by field emission scanning electron microscopy (SEM, Hitachi S-4800, Japan). The crystal structures of as prepared samples were detected by X-ray diffraction (XRD, D8 ADVANCE, Japan) with Cu Kα radiation in the 2θ range from 20° to 70°. UV–vis diffuse reflectance spectra (UV–vis DRS, TU-1901) of the catalysts were recorded to investigate the light absorbance. The generation of hydroxyl radicals (·OH) was detected by fluorospectrophotometer (FL, RF-5301PC, Japan).

2.3 Photocatalytic system and photodegradation experiments

The schematic diagram of the photocatalytic system was shown in Fig.1. The photocatalytic reactors were composed by trilaminar Ti meshes supported TiO_2 (3-TiO_2/TMs), one Ti foil supported TiO_2 (1-TiO_2/TF) and trilaminar Ti meshes supported N-S-C-tridoped TiO_2 nanosheets (3-N-S-C/TiO_2/TMs), respectively. A 500 W xenon lamp with a cut off filter ($\lambda \geq 420$ nm) was used as the visible light source. The distance between two Ti meshes was 1 cm.

In the photodegradation experiment, the photocatalytic activities of catalysts were evaluated by photodegradation of 10 mg L^{-1} norfloxacin solution within 120 min. Prior to irradiation, the catalysts were vertically fixed in a quartz reactor and then stirred in darkness for 30 min to achieve the adsorption/desorption equilibrium. The concentrations of norfloxacin were measured by a Shimadzu LC10A high performance liquid chromatography (HPLC), which was equipped with a Kromasil KR100-5 C18 column. The mobile phase was consisted of a mixture of 87% acetonitrile and 13% of 0.025 mol L^{-1} phosphoric acid solution. The flow rate of mobile phase was 1.0 mL min^{-1}. The absorption wavelength was selected as 276 nm and the injection volume was 20 μL for norfloxacin.

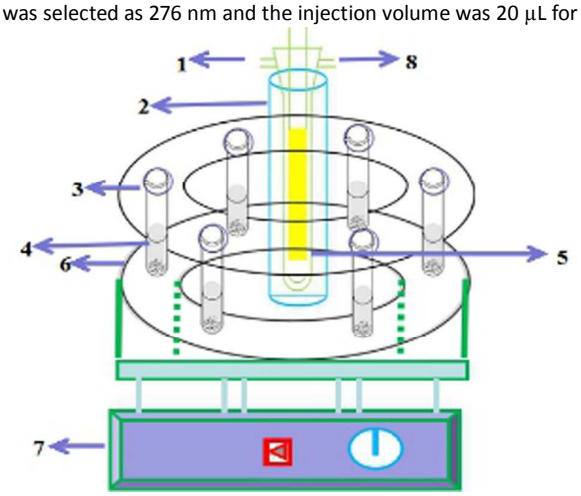

Fig. 1 Schematic diagram of the photocatalytic system. (1) Cooling water entrance; (2) quartz immersion well; (3) quartz reactor; (4) photocatalyst; (5) xenon lamp; (6) magnetic stirrer; (7) photoreactor controller; (8) cooling water outlet.

3. Results and discussion

3.1. XPS analysis

XPS spectra of the obtained samples were performed to investigate the chemical states of doped elements (Fig.2). As displayed in Fig. 2a, three constituents were found in C 1s XPS spectra at around 284.6 and 288.8 eV. The peak at 284.6 eV (C-C) could be assigned to hydrocarbons which arose from residue organics of the sample as well as adventitious carbon absorbed on the surface of the sample, whereas the peaks at 288.8 eV (O-C=O) suggested the substitution of Ti atom by C and the formation of Ti-O-C structure.[30,31] In Fig. 2b, the N 1s peak was divided into two

different peaks at 399.5 and 401.5 eV. The former peak was assigned to O-Ti-N on account of the substitution of some lattice oxygen sites by nitrogen. The latter peak was ascribed to interstitial nitrogen atoms as Ti-O-N structural characteristic in the lattice of N-S-C/TiO_2/TM sample.[32,33] Fig. 2c showed the S 2p XPS peak centered at 168.3 eV. It could be assigned to S^{6+} species in the lattice replaced for Ti^{4+}, indicating the the formation of Ti-O-S bond in the lattice of TiO_2.[34] The XPS spectra analysis results suggested that N, S and C incorporated into the crystal lattice of TiO_2.

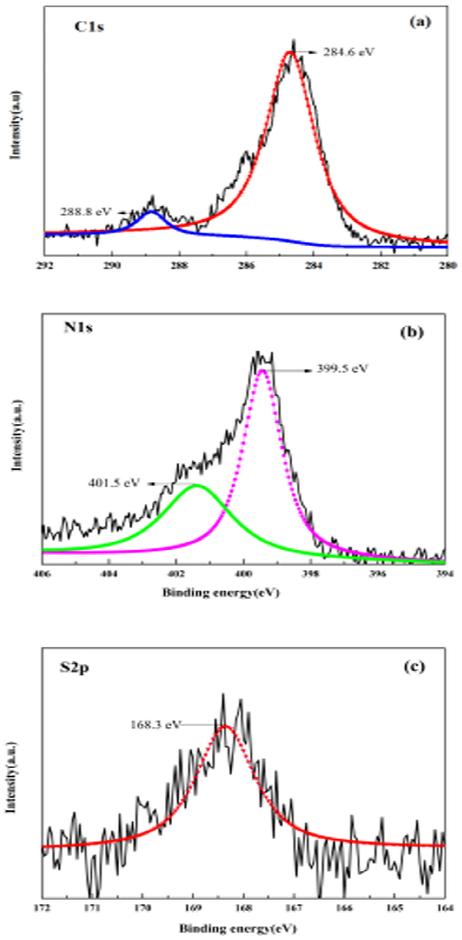

Fig. 2 XPS spectra of (a) C 1s, (b) N 1s and (c) S 2p regions for N-S-C/TiO_2/TM sample.

3.2. Measurement of SEM and XRD

The SEM images of Ti mesh and N-S-C/TiO_2/TM photocatalyst were shown in Fig. 3. The average diameter of N-S-C/TiO_2/TM (0.13 mm) was thicker than that of Ti mesh whose diameter was 0.11 mm (Fig. 3a, b), suggesting that N-S-C-tridoped TiO_2 nanosheets were formed on the surface of Ti mesh. In Fig. 3b, the average area of rectangle hole was observed and evaluated to be 0.0528 mm^2, which could provide a large superficial area for light to pass through in the photocatalytic reaction. It was worth mentioning that amounts of protuberant spherical N-S-C-tridoped TiO_2 nanosheets were observed on the surface of Ti wire (Fig. 3b,c). The magnified SEM image of N-S-C/TiO_2/TM sample in Fig. 3c showed that the spherical nanosheets were grown radially in all directions over the Ti wire. Unlike planar Ti foil where nanosheets were grown vertically in 2D arrays, N-S-C-tridoped TiO_2 nanosheets arrays grown on Ti wires were radially extended in 3D arrays. It could be expected that such a 3D mesh might possess a more excellent photocatalytic activity than that of a 2D foil, which would be discussed later. As shown in Fig. 3d, the spherical N-S-C-tridoped TiO_2 nanosheets displayed beautifully in a pattern of a flower with the width of the nanosheets ranging from ca. 100 to 600 nm and wall thickness of approximately 12 nm.

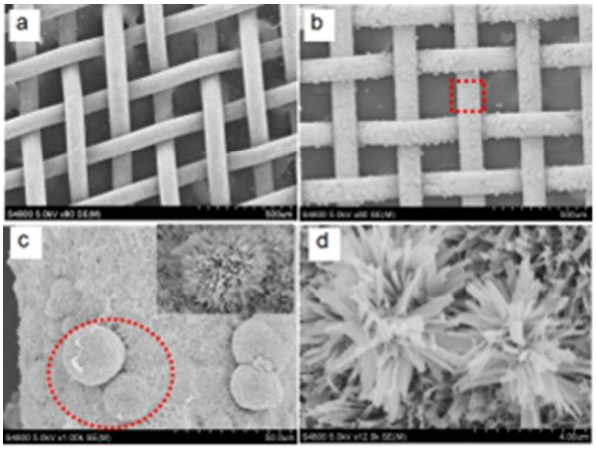

Fig. 3 SEM images of (a) Ti mesh, (b-d) N-S-C/TiO_2/TM photocatalyst.

Fig. 4 showed the XRD patterns of Ti mesh, TiO_2/TM and N-S-C/TiO_2/TM samples. Several characteristic peaks appeared at 25.7°, 48.5°, 54.3° and 55.5° could be observed in the TiO_2/TM and N-S-C/TiO_2/TM samples, corresponding to the (101), (200), (105) and (211) crystal planes of anatase TiO_2, respectively (JPCDS No. 21-1272). And no signal related to rutile phase was appeared in both TiO_2/TM and N-S-C/TiO_2/TM samples due to the insufficient annealing temperature.[35] Generally, the crystalline anatase phase was considered as the most active form of TiO_2 in photocatalytic reaction.[36] The crystallite sizes of the samples could be estimated from the broadening of the corresponding X-ray spectral peak according to Scherrer formula.[37] It was calculated that TiO_2/TM has an average crystallite size of 38.8 nm and it decreases up to 31.2 nm for N-S-C/TiO_2/TM. This observation indicated that the tridoping of N, S and C inhibited grain growth, which was consistent with the previous reports.[38]

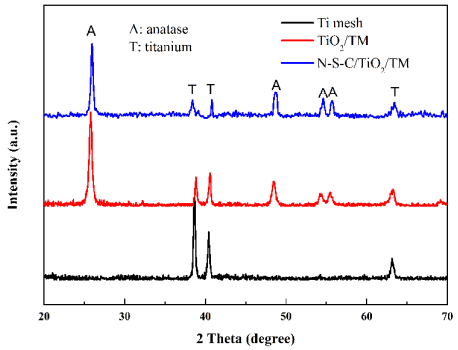

Fig. 4 XRD spectra of Ti mesh, TiO_2/TM and N-S-C/TiO_2/TM samples.

3.3. UV-vis DRS analysis

The optical property of the as-synthesized N-S-C/TiO_2/TM photocatalysts, together with the TiO_2/TM, had been measured by UV-visible diffuse reflectance spectra (DRS). As displayed in Fig. 5, both undoped and N-S-C-tridoped TiO_2/TM samples presented broad light absorption in visible light region from 400-800 nm. The result was possibly caused by the trapped charge carriers, some colored centers or/and the absorption of incident light by the nanosheets.[39,40] Furthermore, the N-S-C/TiO_2/TM sample obviously have the stronger absorption to the visible-light. The result could be attributed to the tridoping of N, S and C elements, which narrowed the band-gap of the TiO_2 and produced more charge carriers.[41] The band-gap energies of TiO_2/TM and N-S-C/TiO_2/TM could be calculated by using Kubelk-Munk function.[42] The relation between the absorption coefficient (α) and incident photon energy (hν) could be written as $\alpha=B_i(h\nu-Eg)2/\lambda$, where α was the absorption coefficien; B_i was the absorption constant for indirect transitions; $h\nu$ represented the discrete photon energy; λ was the wavelength.[43] Plots of $(\alpha h\nu)^{1/2}$ versus $h\nu$ from the spectral data were shown in the inset in Fig. 5. As expected, the band-gap of TM was 3.01 eV, which was consistent with the relatively weak visible-light absorbance ability. For N-S-C/TiO_2/TM sample, the band-gap energy

was reduced to 2.41 eV, suggesting that the tridoping of N, S and C elements narrowed the band gap energy of TiO_2/TM, which should give rise to the occurrence of the hybridized states located in the band-gap.[44]

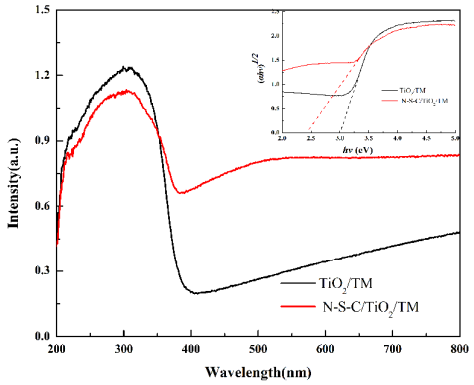

Fig. 5 Optical absorbance spectra of bare and N-S-C-tridoped TiO_2/TM photocatalysts.

3.4. Photocatalytic activities

The photocatalytic activities of 1-TiO_2/TF, equiponderant 3-TiO_2/TMs and 3-N-S-C/TiO_2/TMs were evaluated by degradation of 10 mg L^{-1} norfloxacin under visible light irradiation. As shown in Fig. 6, the corresponding degradation values were 23% and 55% for the 3-TiO_2/TMs and 1-TiO_2/TF catalysts, respectively. Compared with 1-TiO_2/TF, about 32% improvement was achieved by 3-TiO_2/TMs when equiponderant metallic Ti was used. The result mainly attributed to the 3D nanosheets structure and improved optical energy utilization of TiO_2/TM, which would be discussed later. Compared to 3-TiO_2/TMs, the 3-N-S-C/TiO_2/TMs catalysts revealed the significantly higher photocatalytic efficiency with 92% of norfloxacin could be decomposed, which could be ascribed to the intensive visible light absorbance of N-S-C/TiO_2/TM. The initial degradation kinetics of TiO_2 photocatalysis often obeyed pseudo-first-order kinetics function.[45] The linear relationships of -ln(C/C_0) versus reaction time as well as the corresponding rate constants were shown in the insert of Fig. 6. The rate constants of 1-TiO_2/TF, 3-TiO_2/TMs and 3-N-S-C/TiO_2/TMs were 0.0020, 0.0059 and 0.0179 min^{-1}, respectively. Obviously, the kinetic constants of 3-TiO_2/TMs was approximately three times than that of 1-TiO_2/TF. Moreover, the 3-N-S-C/TiO_2/TMs presented the best phtocatalytic activity, which was consistent with the previous analysis.

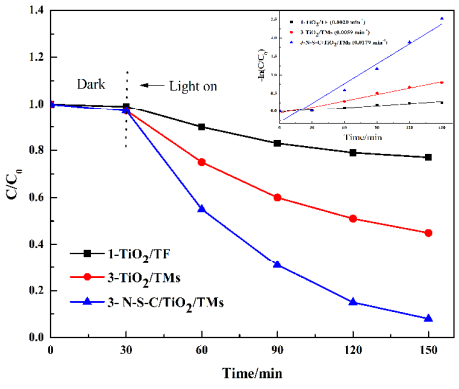

Fig. 6 Photodegradaton efficiency of norfloxacin solution over the as-fabricated catalysts under visible-light irradiation.

Hydroxyl radical (•OH) was recommended as the primary reactive species in driving photocatalytic oxidation processes.[46] To further study the photocatalytic properties of the reaction systems, FL technique with terephthalic acid (TA) as the probe was applied to detect the yield of •OH radicals. The method was based on the characteristic

fluorescence of 2-hydroxyterephthalic acid (TAOH) which was generated by the reaction of •OH radicals and TA.[47] Fig. 7 showed the comparison of FL intensity of TAOH with the visible-light irradiation. There was no •OH in the system containing one Ti mesh, demonstrating that •OH radicals was produced by TiO_2. The 3-TiO_2/TMs revealed a stronger FL intensity as compared to equiponderant 1-TiO_2/TF, implying that the yield of •OH radicals on 3-TiO_2/TMs was higher than that of 1-TiO_2/TF. The 3-N-S-C/TiO_2/TMs displayed the most production of •OH among all of the prepared catalysts, suggesting the tridoping of N, S and C significantly enhanced the photocatalytic activity of the TiO_2 catalysts.

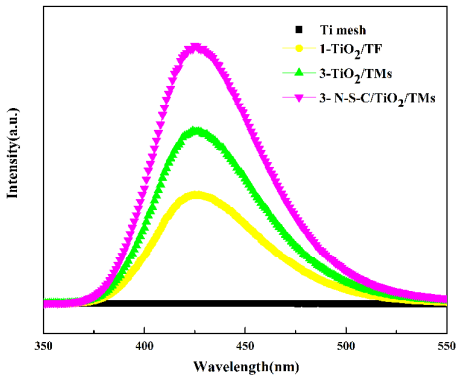

Fig. 7 FL pattern of the as-prepared samples.

To investigate the stability and recyclability of the photocatalysts, the photocatalytic degradation of norfloxacin was carried out for 6 times under visible-light irradiation. As shown in Fig. 8, the degradation rates of norfloxacin by 3-N-S-C/TiO_2/TMs, 3-TiO_2/TMs and 1-TiO_2/TF were decreased approximately 3%, 3% and 4%, respectively. The photocatalytic activities of all the catalysts were slightly decreased, indicating that the catalysts had excellent photocatalytic stability for practical application.

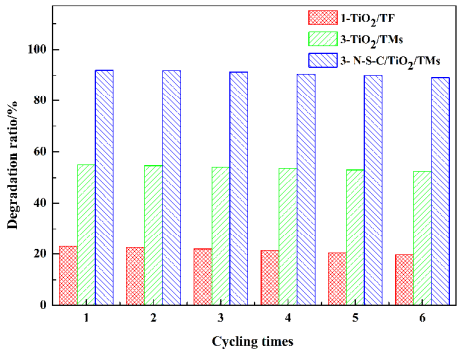

Fig. 8 The recycling times for photodegradation of norfloxacin by different photocatalysts under visible-light irradiation.

3.5. Photocatalytic mechanisms

Several oxidation species, such as •OH, $•O^{2-}$ and h^+, were usually responsible for photocatalytic process.[48] In order to detect the contribution of main active species on the 3-N-S-C/TiO_2/TMs photocatalytic efficiency, tert butyl alcohol (TBA), benzoquinone (BQ) and ammonium oxalate (AO) were selected as the scavengers of •OH, $•O^{2-}$ and h^+, respectively. Fig. 9 showed the photocatalytic activity of 3-N-S-C/TiO_2/TMs under the different conditions. The photocatalytic efficiency decreased with the addition of scavengers, which confirmed the existance of •OH, $•O^{2-}$ and h^+ during the photocatalytic process. The degradation of norfloxacin was sharply decreased from 92% to 16% with the addition of TBA. Furthermore, the addition of BQ and AO could also inhibit the degradation of norfloxacin moderately. Thus, it could be concluded that each reactive species played important role in controlling the

photocatalytic activities, and the participation of •OH radicals was mainly responsible for the photocatalytic reactions.

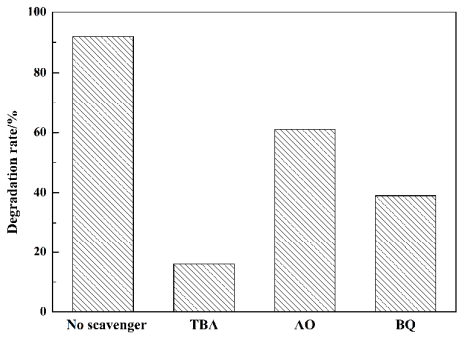

Fig. 9 Effect of radical scavengers on photocatalytic degradation of norfloxacin by 3-N-S-C/TiO_2/TMs.

The schematical representation of the improvement in optical utilization and photocatalytic activity of 3-TiO_2/TMs was shown in Fig. 10a. According to the above analysis, 3-TiO_2/TMs possessed the better photocatalytic activity than that of 1-TiO_2/TF when the equiponderant metallic Ti was used. The result could be attributed to the particular geometry of the 3-TiO_2/TMs catalysts as following. First, unlike two-dimensional TiO_2 nanosheets prepared on planar Ti foil, the Ti mesh supported nanosheets extending radically in a 3D array on a grid of Ti wires, leading to a more efficient absorbance of scattered radiation. Therefore, the loss of photos induced by scattering effects in the reaction liquid could potentially be minimized due to the nanosheets could absorb reflected and refracted light. Moreover, the network structure of TiO_2/TM was also in favor of optical utilization in the reaction system. As seen, part of the incident light could traverse the units of the former TiO_2/TM and be utilized by the latter. At the same time, the reflected and refracted light occurred on the latter TiO_2/TM could back to the rear of the first TiO_2/TM and be reutilized as incident light. Thus, comparing to the equiponderant Ti foil, the network structure of Ti meshes could effectively enhanced the photons utilization in the photocatalytic reaction. In addition, the prominent spherical TiO_2 nanosheets most probably allowed norfloxacin molecules more easily to access the photocatalyst surface, which contributed to enhancing the photocatalytic activity of catalysts as well.

The enhanced photocatalytic mechanism for the N-S-C/TiO_2/TM sample was shown in Fig. 10b. With the incorporation of N, S and C into TiO_2 lattice, new impurity levels including the N 2p gap level above the O 2p valence band (VB), S 2p and C 1s gap levels under the Ti 3d conduction band (CB) could be formed.[49-51] The new S 2p and C 1s levels of N-S-C/TiO_2/TM served as trapping centers for photogenerated electrons, which could promote the separation of electrone-hole pairs and enhance the lifetime of charge carriers. The photoinduced electrones (e^-) could be excited and migrated from the N 2p level to CB, S 2p and C 1s levels under visible-light irradiation. The holes (h^+) on the N 2p level could transfer to the surface of catalyst and oxidize H_2O molecules and OH^- to •OH radicals. In addition, the CB electrons and trapped electrons could trap the adsorbed O_2 molecules to generate $•O^{2-}$, and further form the high active species of •OH radicals. As a result, norfloxacin molecules in the aqueous solution were mineralized by the •OH radicals into CO_2, H_2O and other products.

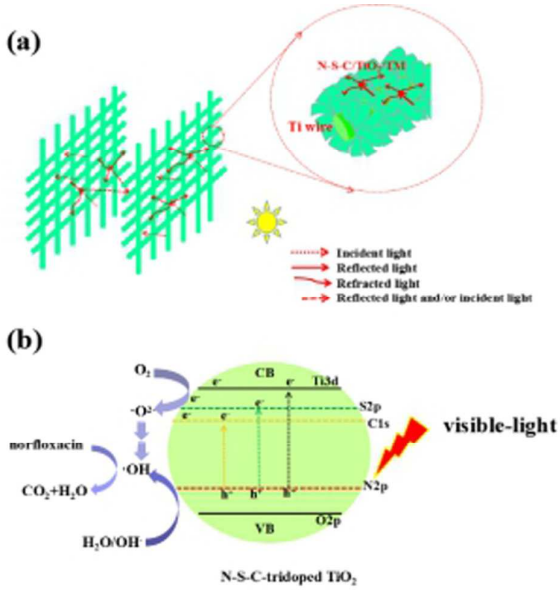

Fig. 10 Schematical representation of the improvement in the photoactivity of (a) 3-TiO_2/TMs and (b) N-S-C/TiO_2/TM catalysts.

4. Conclusions

The N-S-C-tridoped TiO_2/TMs photocatalysts were successfully fabricated via one-step hydrothermal synthesis in the mixture of sodium hydroxide and cystine, and followed by acid-washing and calcination. The tridoping of N, S and C significantly enhanced the visible-light absorption and photocatalysis of TiO_2/TM. Furthermore, compared with the equiponderant 1-TiO_2/TF catalyst, the mesh catalysts of 3-TiO_2/TMs possessed a 3D TiO_2 nanosheets arrays and high optical energy utilization, which was in favor of the photocatalytic degradation of norfloxacin. Additionally, the enhanced photocatalytic mechanism for N-S-C-TiO_2/TM was discussed in detail.

Acknowledgments

This work was supported by National Natural Science Foundation of China for Youth (21106035) and Youth Scholar Backbone Supporting Plan Project for General Colleges and Universities of Heilongjiang province (1151G034), and Key Laboratory of Chemical Engineering Process & Technology for High-efficiency Conversion (Heilongjiang University), College of Heilongjiang Province.

References

[1] A.L. Giraldo, G.A. Pe nuela, R.A. Torres-Palma, N.J. Pino, R.A. Palominos and H.D. Mansilla, *Water Res.,* 2010, **44,** 5158.
[2] L.V.D.S. Santos, A.M. Meireles and L.C. Lange, *J. Environ. Manage.,* 2015, **154,** 8.
[3] S. Garnayak and S. Patel, *J. Mol. Liq.,* 2015, **209,** 327.
[4] J.S. Solomkin, H.H. Reinhart, E.P. Dellinger, et al., *Ann. Surg.,* 1996, **223,** 303.
[5] R. Davis, A. Markham and J.A. Balfour, *Drugs,* 1996, **51,** 1019.
[6] C. Marta, Francisco, Omil, J.M. Lema, L María and G.J. Carmen, *Water Res.,* **2004,** 38, 2918.
[7] G. Meritxell, P. Mira, G. Antoni and B. Damià, *Environ. Int.,* 2010, **36,** 15.
[8] R.H. Lindberg, P. Wennberg, M.I. Johansson, M. Tysklind and B.A.V. Andersson, *Environ. Sci. Technol.,* 2005, **39,** 3421.
[9] J.M. Cha, S. Yang and K.H. Carlson, *J. Chromatogr. A,* 2005, **1065,** 187.
[10] A.J. Watkinson, E.J. Murby, D.W. Kolpin and S.D. Costanzo, *Sci. Total Environ.,* 2009, **407,** 2711.
[11] M.J. Chen and W. Chu, *J. Hazard. Mater.,* 2012, **219,** 183.
[12] A. Fujishima and K. Honda, *Nature,* 1972, **238,** 37.
[13] W.S. Tung and W.A. Daoud, *J. Am. Ceram. Soc.,* 2012, **95,** 2330.
[14] I.S. Grover, S. Singh and B. Pal, *Appl. Surf. Sci.,* 2013, **280,** 366.
[15] X.F. Lei and X.X. Xue, *Mater. Sci. Semicond. Process.,* 2008, **11,** 117.
[16] C.C. Hu, T.C. Hsu and S.Y. Lu, *Appl. Surf. Sci.,* 2013, **280,** 171.
[17] X.F. Lei and X.X. Xue, Mater. *Chem. Phys.,* 2008, **112,** 928.
[18] V. Trevisan, A. Olivo, F. Pinna, M. Signoretto, F. Vindigni, G. Cerrato and C.L. Bianchi, *Appl. Catal., B,* 2014, **160,**

152.
[19] J. Lv, T. Sheng, L.L. Su, G.Q. Xu, D.M. Wang, Z.X. Zheng and Y.C. Wu, *Appl. Surf. Sci.* 2013, **284,** 229.
[20] X.F. Lei, X.X. Xue, H. Yang, C. Chen, X.Li, J.X. Pei, M.C. Niua, Y.T. Yang and X.Y. Gao, *J. Alloys Compd.,* 2015, **646,** 541.
[21] G.S. Zhang, Y.C. Zhang, M. Nadagouda, C. Han, K. O'Shea, S.M. El-Sheikh, A.A. Ismail and D.D. Dionysiou, *Appl. Catal., B,* 2014, **144,** 614.
[22] X.W. Cheng, X.J. Yu and Z.P. Xing, *Appl. Surf. Sci.,* 2012, **258,** 7644.
[23] J.A. Byrne, B.R. Eggins, N.M.D. Brown, B. McKinney and M. Rouse, *Appl. Catal., B,* 1998, **17,** 25.
[24] K. Vinodgopal, I. Bedja and P.V. Kamat, *Chem. Mater.,* 1996, **8,** 2180.
[25] D. Li, Z.P. Xing, X.J. Yu and X.W. Cheng, *Electrochim. Acta,* 2015, **170,** 182.
[26] J.J. Liao, S.W. Lin, L. Zhang, N.Q. Pan, X.K. Cao and J.B. Li, *ACS Appl. Mater. Interfaces,* 2012, **4,** 171.
[27] D. Li, X.W. Cheng, X.J. Yu and Z.P. Xing, *Chem. Eng. J.,* 2015, **279,** 994.
[28] Z. Liu, V. Subramania and M. Misra, *J. Phys. Chem., C,* 2009, **113,** 14028.
[29] M.L. Zhong, G.Q. Zhang and X.Q. Yang, *Mater. Lett.,* 2015, **145,** 216.
[30] V. Kiran and S. Sampath, *ACS Appl. Mater. Int.,* 2012, **4,** 3818.
[31] W.J. Ren, Z.H. Ai, F.L. Jia, L.Z. Zhang, X.X. Fan and Z.G. Zou, *Appl. Catal., B,* 2007, **69,** 138.
[32] R. Asahi, T. Morikawa, T. Ohwaki, K. Aoki and Y. Taga, *Science,* 2001, **293,** 269.
[33] Y. Cong, J. L. Zhang, F. Chen and M. Anpo, *J. Phys. Chem., C,* 2007, **111,** 6976.
[34] C. McManamon, J. O'Connell, P. Delaney, S. Rasappa, J. Holmes and M. Morris, *J. Mol. Catal., A,* 2015, **406,** 51.
[35] H.L. Chen, K.F. Chen, S.W. Lai, Z. Dang and Y.P. Peng. *Sep. Purif. Technol.,* 2015, **146,** 143.
[36] M. Janus, J. Zatorska, A.C. Zewski, K. Bubacz, E.K. Nejman and A. Morawski, *Appl. Surf. Sci.,* 2015, **330,** 200.
[37] S. Bangkedphol, H.E. Keenan, C.M. Davidson, A. Sakultantimetha, W. Sirisaksoontorn and A. Songsasen, *J. Hazard. Mater.,* 2010, **184,** 553.
[38] N. Yao, C.C. Wu, L.C. Jia, S. Han, B. Chi, J. Pu and L. Jian, *Ceram. Int.,* 2012, **38,** 1671.
[39] Z.H. Xu and J.G. Yu, *Nanoscale,* 2011, **3,** 3138.
[40] H.F. Zhuang, C.J. Lin, Y.K. Lai, L. Sun and J. Li, *Environ. Sci. Technol.,* 2007, **41,** 4735.
[41] N. Yao, C.C. Wu, L.C. Jia, S. Han, B. Chi, J. Pu and L. Jian, *Ceram. Int.,* 2012, **38,** 1671.
[42] F. Spadavecchia, C. Cappelletti, S. Ardizzone, C.L. Bianchi, S. Cappelli, C. Oliva, P. Scardi, M. Leoni and P. Fermo, *Appl. Catal., B,* 2010, **96,** 314.
[43] X. Song and L. Gao, *Langmuir,* 2007, **23,** 11850.
[44] Y.L. Kuo, T.L. Su, F.C. Kung and T.J. Wu, *J. Hazard. Mater.,* 2011, **190,** 938.
[45] C. Zhao, M. Pelaez, D.D. Dionysiou, S.C. Pillai, J. A. Byrne and K.E. O'Shea, *Catal. Today,* 2014, **224,** 70.
[46] W.J. Li, D.Z. Li, Y.M. Lin, P.X. Wang, W. Chen and X.Z. Fu, *J. Phys. Chem., C,* 2012, **116,** 3552.
[47] K. Ishibashi, A. Fujishima, T. Watanabe and K. Hashimoto, *Electrochem. Commun.,* 2000, **2,** 207.
[48] X.W. Cheng, H.L. Liu, Q.H. Chen, J.J. Li and P. Wang, *J. Hazard. Mater.,* 2013, **254,** 141.
[49] J.C. Yu, W.K. Ho, J.G. Yu, H.P. Yip, P.K. Wong and J.C. Zhao, *Environ. Sci. Technol.,* 2005, **39,** 1175.
[50] X.W. Cheng, X.J. Yu and Z.P. Xing, *J. Colloid Interface Sci.,* 2012, **372,** 1.
[51] H. Kamisaka, T. Adachi and K. Yamashita, *J. Chem. Phys.,* 2005, **123,** 7648.

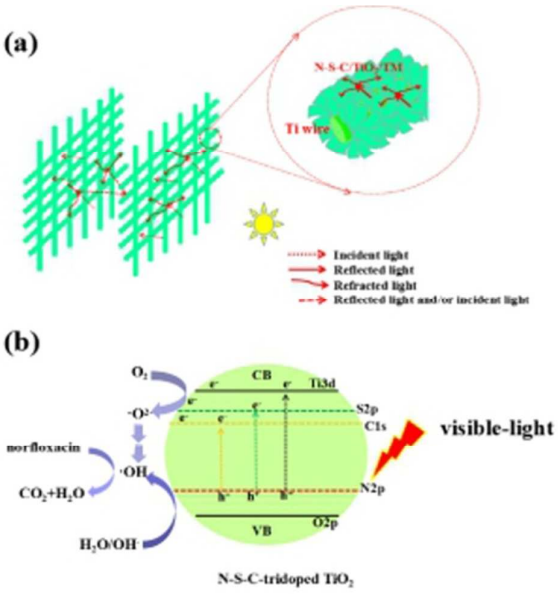
(a)
N-S-C/TiO2-TM
Ti wire
Incident light
Reflected light
Refracted light
Reflected light and/or incident light
(b)
O2
·O2-
norfloxacin
·OH
CO2+H2O
H2O/OH-
CB
Ti3d
S2p
C1s
N2p
VB
O2p
visible-light
N-S-C-tridoped TiO2